

A Parametric Survey of the CME Triggering Process by Numerical Simulations *

Xiao-Yan Xu, Peng-Fei Chen and Cheng Fang

Department of Astronomy, Nanjing University, Nanjing 210093; xyxu@nju.edu.cn

Received 2005 May 19; accepted 2005 July 2

Abstract Observations indicate that solar coronal mass ejections (CMEs) are closely associated with reconnection-favored flux emergence, which was explained in the emerging flux trigger mechanism for CMEs by Chen & Shibata based on numerical simulations. We present a parametric survey of the triggering agent: its polarity orientation, position, and the amount of the unsigned flux. The results suggest that whether a CME can be triggered depends on both the amount and location of the emerging flux, in addition to its polarity orientation. A diagram is presented to show the eruption and non-eruption regimes in the parameter space. The work is aimed at providing useful information for the space weather forecast.

Key words: Sun: coronal mass ejections (CMEs)—Sun: filaments

1 INTRODUCTION

Solar coronal mass ejection (CME) is one of the most violent energy releasing processes on the Sun. A major eruption usually releases more than 10^{32} erg of energy and ejects more than 10^{16} g of solar plasma into the interplanetary space, which may seriously damage satellites as well as disrupt ground communications and power grids. So CME forecast is an important and urgent issue.

Magnetic arcades with shear motion are widely studied in recent years. It is found that after a large enough shear, the closed magnetic arcades would approach an open field, and an eruption may be triggered by resistive instability (e.g. Biskamp & Welter 1989; Finn, Guzdar & Chen 1992; Mikić & Linker 1994). For a pure shear motion, however, it takes an unrealistically long time for the shear to exceed the critical value. Besides, it was found that the magnetic shear in some observational reports is due to the emergence of a twisted flux rope (Kurokawa 1987, 1996). Wu & Guo (1997) indicated that the emergence of a strong enough magnetic bubble below a helmet can destabilize the helmet to form a CME. Before this, Guo, Wu & Tandberg-Hanssen (1996) simulated a similar process but with opposite magnetic field direction in the bubble, and the oppositely-directed magnetic field lines in the bubble reconnect with the magnetic field in

* Supported by the National Natural Science Foundation of China.

the helmet, so as to produce a new magnetic rope, which is similar to the emerging magnetic bubble in Wu & Guo (1997). In both cases, a helmet eruption can be induced.

Emerging flux is probably related to both CMEs and solar flares (Heyvaerts, Priest & Rust 1977; Yokoyama & Shibata 1996; Chen et al. 1999). Observational study by Feynman & Martin (1995) indicated that many CMEs are correlated with emerging flux. Their research also suggested that emerging flux favorable for magnetic reconnection with pre-existing magnetic field has a high probability of triggering filament eruptions, and this was confirmed by Wang & Sheeley (1999). It was found that magnetic cancellation may play a role in CME initiation (Zhang et al. 2001; Zhang & Wang 2001). It is noted that the emerging flux may appear either within or on the outer edge of the filament channel. Chen & Shibata (2000) proposed an emerging flux triggering mechanism for CMEs, which provides a physical explanation for the above observational results. It is further pointed out that inside the filament channel even a small amount of emerging flux may play a role, while on the outer edge of the channel there may exist a threshold for the emerging flux, below which the flux rope can not be triggered and erupt (Chen, Shibata & Yokoyama 2001). Later, using a simple analytic model, Lin, Forbes & Isenberg (2001) and Lin (2002) investigated the correlation between flux emergence and the catastrophe of a flux rope, but failed to find a universal relation.

To confirm the correlation discovered by Feynman & Martin (1995), detailed surveys in both observations and numerical simulations are necessary. In this paper we extend the work of Chen et al. (2001) to present a parametric survey on the condition that CMEs can be triggered. The numerical method is described in Section 2, the numerical results are presented in Section 3, and a discussion and conclusions are given in Sections 4 and 5, respectively.

2 NUMERICAL METHOD

With gravity and heat conduction omitted, the two-dimensional time dependent compressible resistive MHD equations are numerically solved with a multi-step implicit scheme (Hu 1989; Chen, Fang & Hu 2000):

$$\frac{\partial \rho}{\partial t} + \nabla \cdot (\rho \mathbf{v}) = 0, \quad (1)$$

$$\frac{\partial \mathbf{v}}{\partial t} + (\mathbf{v} \cdot \nabla) \mathbf{v} + \frac{1}{\rho} \nabla P - \frac{2}{\rho \beta_0} \mathbf{j} \times \mathbf{B} = 0, \quad (2)$$

$$\frac{\partial \psi}{\partial t} + \mathbf{v} \cdot \nabla \psi - \eta \Delta \psi = 0, \quad (3)$$

$$\frac{\partial T}{\partial t} + \mathbf{v} \cdot \nabla T + (\gamma - 1) T \nabla \cdot \mathbf{v} - \frac{2(\gamma - 1)\eta}{\rho \beta_0} \mathbf{j} \cdot \mathbf{j} = 0, \quad (4)$$

where $\gamma=5/3$ is the ratio of specific heats; the five independent variables are the density (ρ), velocity (v_x, v_y), magnetic flux function (ψ), and temperature (T). The magnetic flux function ψ is related to the magnetic field (\mathbf{B}) by $\mathbf{B} = \nabla \times (\psi \hat{e}_z)$. Here $\mathbf{j} = \nabla \times \mathbf{B}$ is the current density. Characteristic values for ρ and T are $\rho_0 = 1.67 \times 10^{-12} \text{ kg m}^{-3}$ and $T_0 = 10^6 \text{ K}$. The corresponding Alfvén speed v_A is 1381 km s^{-1} if β_0 is chosen to be 0.01. As indicated in Chen et al. (1999), the dimensionless results are independent of the length scale when gravity is neglected.

Here we may take the length scale $L_0 = 2.0 \times 10^4 \text{ km}$, hence an Alfvén transit time τ_A ($= L_0/v_A$) equals to 14.5 s. The resistivity η , which is distributed outside the initial current filament, has the following dependence on the current-density j_z :

$$\eta = \begin{cases} \eta_0 \min(1, |\frac{j_z}{j_c}| - 1), & |j_z| \geq j_c; \\ 0 & |j_z| < j_c, \end{cases} \quad (5)$$

where $\eta_0 = 0.02$, and $j_c = 0.5$ is the critical value of j_z , beyond which the resistivity is assumed to be excited (Chen & Shibata 2000).

The initial magnetic configuration is a flux rope surrounded by a quadrupolar field as used by Chen & Shibata (2000), which is expressed as $\psi = \psi_b + \psi_i + \psi_l$, where the background field (ψ_b), the magnetic components of the image current (ψ_i) and the line current (ψ_l) have the following forms:

$$\psi_b = c \ln \frac{[(x + 0.3)^2 + (y + 0.3)^2][(x - 0.3)^2 + (y + 0.3)^2]}{[(x + 1.5)^2 + (y + 0.3)^2][(x - 1.5)^2 + (y + 0.3)^2]}, \quad (6)$$

$$\psi_i = -\frac{r_0}{2} \ln[x^2 + (y + h)^2], \quad (7)$$

$$\psi_l = \begin{cases} r^2/(2r_0), & r \leq r_0; \\ r_0/2 - r_0 \ln(r_0) + r_0 \ln(r), & r > r_0. \end{cases} \quad (8)$$

The coefficient c in Eq. (6) represents the strength of the background field, and is determined by trial and error in order to guarantee that the center of the flux rope remains stable for long enough time during the numerical simulation. In our simulations presented here, c is set at 2.5526, $r = [x^2 + (y - h)^2]^{1/2}$, $h = 2$, and $r_0 = 0.5$. In this configuration, the magnetic field (\mathbf{B}) decreases as $\sim y^{-3}$ along the height y . The initial conditions of other quantities are the same as that in Chen & Shibata (2000).

The dimensionless size of the simulation box is $-12 \leq x \leq 12$ and $0 \leq y \leq 18$. The domain is divided by 161×181 grid points, which are uniformly distributed in the y -direction and non-uniformly along the x -direction. The bottom of the simulation area is a line-tying boundary, where all quantities except T are fixed. Outside the flux emerging region, T is determined by equivalent extrapolation. The other three boundaries are assumed to be open ones. The flux emergence is realized by changing the boundary magnetic field. Here we change the value of ψ until $t = t_e = 100 \tau_A$, i.e., $\psi(x, 0, t) = \psi(x, 0, 0) + \psi_e t/t_e$ ($t \leq t_e$), where $\psi_e = A \cos(\pi(x-d)/0.6)$ is distributed in the local region $|x - d| \leq 0.3$ with d representing the location of the emerging flux. In the magnetic configuration considered in this paper, the width of filament channel is within a distance d to the magnetic neutral line, $|d| = 1.0$ (in units of $L_0 = 2.0 \times 10^4$ km). After $t = t_e$, the bottom boundary is fixed as before.

In our parametric survey, the emerging flux is characterized by three free parameters: the amount of the total flux, the central location (d), and the polarity orientation (i.e., the sign of A). For simplicity, the length of the filament channel is taken to be 10 times larger than its width, the amount of the emerging flux is thus $10|A|B_0(L_0)^2$ in our 2D simulation, which varies from 10^{19} Mx to 10^{21} Mx, typical values for newly emerging flux (Tang et al. 2003; Wang et al. 2004).

Owing to the unavoidable numerical diffusion, the initial quasi-equilibrium can not last forever, which makes it difficult to distinguish an eruption case from a non-eruption case near the critical regimes. Here, the eruption case is determined when the following criteria are satisfied:

- (1) Near $t = 50\tau_A$, the velocity of the flux rope $v > 5v_0$, where v_0 is the velocity of the flux rope when the initial state evolves without any perturbation;
- (2) The maximum velocity of the eruptive flux rope v_{\max} is larger than $v_{\max 0}$, where $v_{\max 0}$ is the maximum velocity of the flux rope in the zero-perturbation evolution;
- (3) $t_{\max} < t_{\max 0}$, where t_{\max} is the time when the velocity of the eruptive flux rope reaches maximum within $200 \tau_A$, and $t_{\max 0}$ the counterpart of the zero-perturbation evolution.

3 NUMERICAL RESULTS

Emerging flux may have the same or opposite polarity orientation as the ambient magnetic field of the filament. So two categories of emerging flux were distinguished in our numerical simulations. In Category A, the emerging flux is located at the outer edge of a filament channel ($|d| > 1.0$), and has the same polarity orientation as the ambient magnetic field of the flux rope (clockwise), as shown in Figures 1a and 2a. We formulate the emerging flux in Category A by $\psi_e = -A \cos(\pi(x-d)/0.6)$, where A is a constant ranging from 1 to 25, depending on the flux, and d is the distance from the axis of the emerging flux to the magnetic neutral line ($d = 0$). We take $|x-d| \leq 0.3$. In Category B the emerging flux is within the filament channel ($|d| \leq 1.0$) or near one side of the filament channel, and has the opposite polarity orientation (anticlockwise) to the ambient magnetic field of the flux rope, as shown in Figures 1b and 2b. The emerging flux is represented as $\psi_e = A \cos(\pi(x-d)/0.6)$ in this case. We investigate the response of a flux rope system to an emerging flux, taking the amount and location of the emerging flux as free parameters.

Our results of numerical simulations are displayed in Figure 3, where only emerging flux with the parameters (location and amount) in the “+” regimes can make a flux rope lose its equilibrium and so trigger the onset of a CME. In Figure 3 the upper “+” regime corresponds to the eruptive type of Category A, as shown in Figure 4, and the lower “+” regime, to the eruptive type of Category B, as shown in Figure 5. In Figures 4 and 5, the temperature is shown by the grey scale, the velocity by the arrows, and the magnetic field by solid lines. Our detailed results are as follows:

For the Category A:

In this case, our results indicate that when the emerging flux is located in $|d| < 3.2$ or $|d| > 5.4$, it can not trigger the onset of a CME, and the flux rope may even go downward sometimes, as shown in Figures 6 and 7. On the other hand, when the newly emerging flux is

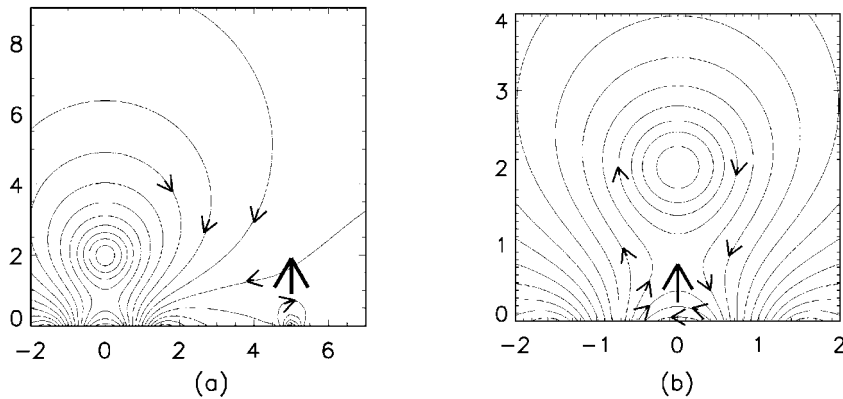


Fig. 1 Schemata showing (a) Category A, which corresponds to the emerging flux located on the outer edge of a filament channel, and with the same polarity orientation (clockwise) as the ambient magnetic field of the flux rope; (b) Category B, where the emerging flux is within the filament channel, and has the opposite polarity orientation (anticlockwise) to the ambient magnetic field of the flux rope. The x -axis is the distance from the magnetic neutral line, the y -axis is the height, both in units $L_0 = 2 \times 10^4$ km. The new magnetic flux emerges along the direction of the thick arrow.

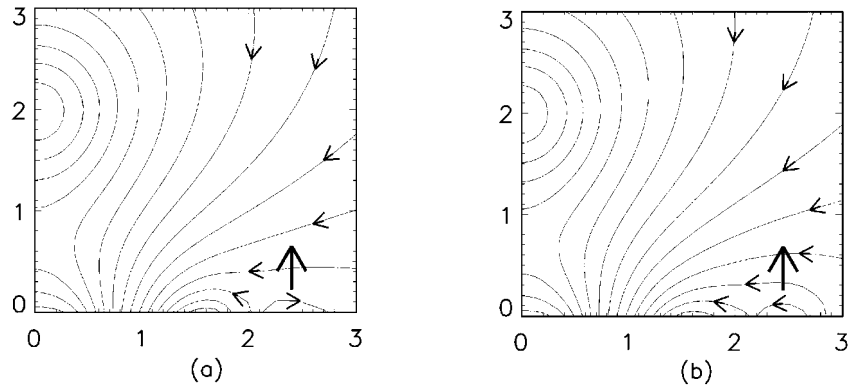


Fig. 2 Sketch showing the cases in the Category B with the emerging flux near one side of the filament channel, with the same polarity orientation (a), and with an opposite one (b) as the ambient magnetic field of the flux rope (clockwise). The new magnetic flux emerges along the direction of the thick arrow.

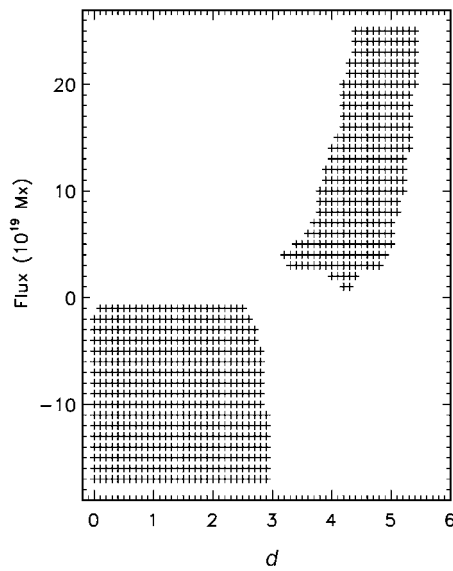


Fig. 3 A plot in the parameter space of the amount of the emerging flux on the outer edge of filament channel or within the channel and its location relative to the magnetic neutral line. Emerging flux with parameters in the “+” regimes is most favorable to trigger the onset of CME.

located in $3.2 \leq |d| \leq 5.4$, then an adequate amount of magnetic flux can cause the flux rope to lose equilibrium and so trigger the eruption of a CME, as shown in Figure 4.

For the Category B:

Almost all emerging flux of this case at the location of $|d| > 3.0$ can not make the flux rope erupt, though A varies over the range from 1 to 25. However, at the location of $|d| < 3.0$, most

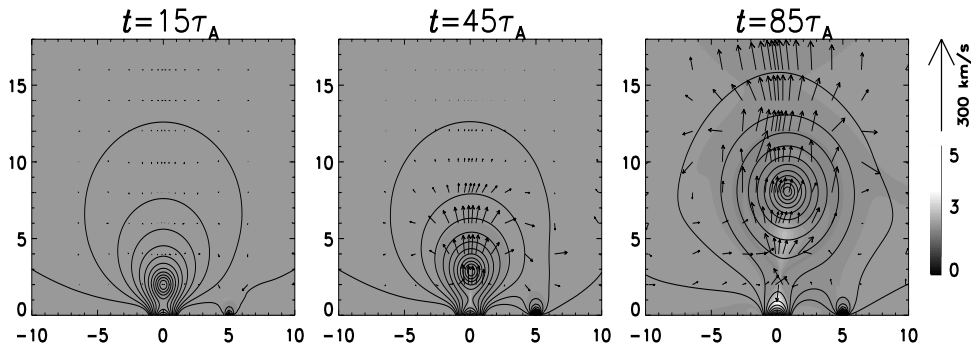


Fig. 4 An example of eruption where the flux rope loses equilibrium after reconnection between the emerging flux on the outer edge of the filament channel and the ambient magnetic field of the flux rope, and is then ejected as reconnection proceeds in the current sheet below. The new magnetic flux emerges in the upper “+” regime in Fig. 3.

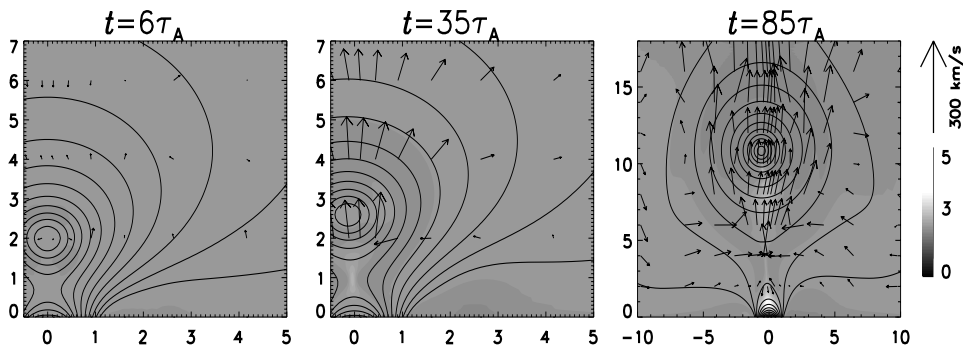


Fig. 5 Another example of eruption where the flux rope loses its equilibrium after reconnection between the emerging flux near the filament channel and the ambient magnetic field of the flux rope, and then is ejected. The new magnetic flux emerges in the lower “+” regime of Fig. 3.

of the emerging flux even with a value of 1.0×10^{19} Mx can make the flux rope lose equilibrium, as shown in Figure 5, except when $|d|$ approaches 3.0, then more flux depending on the location is needed to trigger the eruption. At the magnetic neutral line ($d = 0$), if the emerging flux is less than 2.0×10^{19} Mx, then eruption can not be triggered. It should be emphasized that when the flux emerges near the filament channel ($1.0 < |d| < 3.0$), as shown in Figure 2b, it can also trigger the flux rope to erupt, which will be discussed in Section 4.

Moreover, our numerical simulations indicate that even for the eruption cases the velocity evolution could be different. Although for the different cases there is a common acceleration phase before the velocity maximum, the evolution patterns are different. In our simulations both in Categories A and B, the eruptive ropes near the solar surface have velocities from 40 km s^{-1} to 70 km s^{-1} . This is comparable with the observational results given by Zhang et al. (2001).

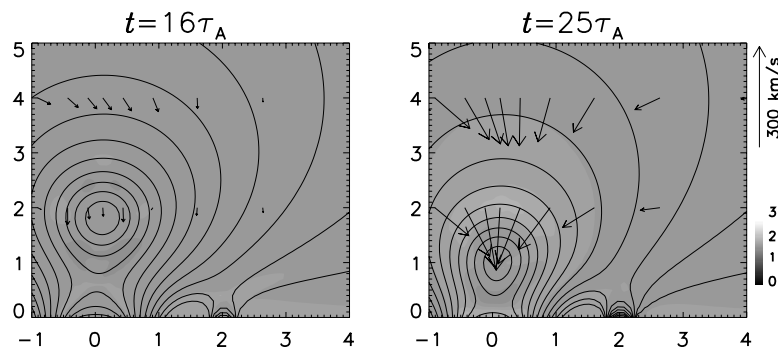


Fig. 6 A non-eruption example where the emerging flux coming out of the filament channel is too close to the magnetic neutral line. The new magnetic flux emerges at the left side of the upper “+” regime in Fig. 3, and can not trigger the eruption of a CME.

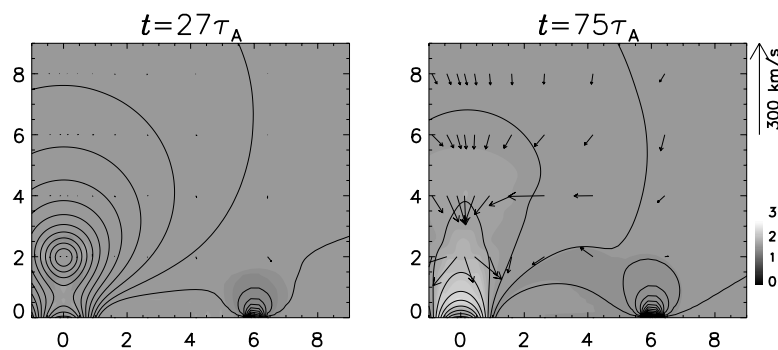


Fig. 7 A non-eruption example where the emerging flux coming out of the filament channel is too far from the magnetic neutral line. The new magnetic flux emerges at the right side of the upper “+” regime in Fig. 3, and can not make a flux rope lose equilibrium leading to a CME.

4 DISCUSSION

Observations have suggested that two categories of emerging flux with reconnection-favored direction can trigger filament eruptions leading to CMEs (Feynman & Martin 1995). The first one is located on the outer edge of the filament channel, and the second is within the channel. Both cases have been verified by Chen & Shibata (2000). Our results indicate further that the eruption can be triggered only if the parameters of the emerging flux including both the location and the amount of the flux are adequate

As shown in Figure 1a for the Category A, when the emerging flux with the same polarity orientation (clockwise) as the ambient magnetic field of the flux rope is located adequately on the outer edge of the filament channel, it can reconnect with the overlying magnetic field. After the reconnection, two laterally interacting magnetic loops evolve to one small inner loop and one large outer loop, as shown in Figure 4, and lead to magnetic cancellation in part, which restructures the pre-existing magnetic configuration and makes the magnetic tension to decrease directly. Then the magnetized plasma mostly at the side of the emerging flux is pressed by the resulting magnetic pressure gradient and moves towards the place of reconnection. The frozen-

in field lines accumulate to form a current sheet (Chen & Shibata 2000). At the same time the locally concave outer loop is ejected outward along with the reconnection outflow, which makes the flux rope lose equilibrium and pushes it upward with a non-perpendicular motion, leading to the onset of flux rope eruption and then a CME. To some extent, the eruption is not directly above the magnetic neutral line, rather, it departs somewhat from the vertical direction, as shown in Figure 4. However, according to our numerical simulation, if the magnetic flux emerges at a place too close to one side of the filament channel, corresponding to left side of the upper “+” regime in Figure 3, it can not trigger the eruption shown in Figure 6. This is due to the fact that the reconnected outer loop becomes scarcely less bent and the magnetic tension only decreases a little after the reconnection, so that the decreased magnetic tension is not enough to make the flux rope lose equilibrium and accelerate upward (Chen & Shibata 2000). On the other hand, if the emerging flux is located too far from the filament channel, which corresponds to the right side of the upper “+” regime in Figure 3, it can not trigger eruption either, as shown in Figure 7. This is due to the fact that the reconnected outer loop has hardly changed, and the magnetic tension has scarcely decreased. Of course, if the emerging flux is located further far away from the filament channel, then there will not be any reconnection at all, and no effect on the filament.

For Category B, the emerging flux is located within or near one side of the filament channel and has the opposite polarity orientation (anticlockwise) to the ambient magnetic field of the flux rope, as shown in Figures 1b and 2b, respectively. In Figure 1b, the emerging flux will continue to reconnect with the bottom part of the ambient coronal magnetic loops (its two “shoulders”), and result in more and more line-tied field lines detached from the solar surface (Chen & Shibata 2000). Therefore, the flux rope loses equilibrium due to the loss of the line-tied constraint and accelerates upward, then ejects away along a nearly perpendicular direction. According to our results, in this case, a flux greater than 1×10^{19} Mx is sufficient to make the filament erupt, except for the center of the filament channel, where a greater flux is needed to trigger the onset. In these situations, if the emerging flux is not strong enough, there is only a few line-tied field lines detached from the solar surface, and the flux rope can not get rid of the line-tied constraint, and thus can not lose equilibrium in the end. It should be mentioned that our results also indicate that, for the same amount of emerging flux, the acceleration of the flux rope is usually larger in Category B than in Category A.

One case shown in Figure 2b in Category B should be pointed out, where the flux emerges near one side of the filament channel ($1.0 < |d| < 3.0$) and can trigger the eruption, as shown in Figure 5. In this case, the magnetic field of the flux reconnects with the low-lying small ambient magnetic loop of the flux rope, then a bigger loop forms, pushes the magnetic field upwards and causes finally the eruption. If, on the contrary, the emerging flux has the same polarity orientation (clockwise) as the ambient magnetic field of the flux rope as shown in Figure 2a, then reconnection will make the magnetic field lines to close up and so will not trigger an eruption (see Fig. 6).

It can be seen in Figure 3 that either on the outer edge of the filament channel or within the channel, not all the emerging flux can make a flux rope (filament) lose equilibrium so leading to the onset of a CME. The minimum value of the newly emerging flux which can trigger an eruption of a flux rope is about 1×10^{19} Mx. Moreover, the location of the emerging flux is also an important parameter. Only the emerging flux with adequate parameters in the “+” regimes shown in Figure 3 can trigger eruption of flux rope. Thus, according to our results, whether a CME can be triggered depends on both the amount and location of the emerging flux. An adequate combination of the two is required. At some adequate locations, the emerging flux with an enough amount can trigger the onset of a flux rope. For the same amount of the emerging flux, however, only emerging fluxes at appropriate locations can trigger an eruption. Our numerical simulations may provide useful information for space weather forecast and give some suggestions

to observers. However, it should be pointed out that our results are only qualitative, because it depends on the detailed magnetic configuration. Further work is necessary to explore the universal role of the emerging flux.

5 SUMMARY

We have numerically investigated the response of a flux rope to magnetic flux emergence. The main results are as follows:

Not all emerging fluxes can make a flux rope (filament) to lose equilibrium and so trigger the onset of a CME. Figure 3 in this paper illustrates the parameter regimes in which the emerging flux can lead to an eruption. It is also indicated that near one side of the filament channel ($1.0 < |d| < 3.0$), only when the emerging flux has the opposite polarity orientation as the ambient magnetic field of the filament channel can an eruption be triggered. Another point is that flares are mostly not just located at the center of CMEs, which is consistent with the results of Harrion (1986).

The results presented in this paper may provide useful information for the space weather forecast, and their validity needs to be verified by observations. The observational examples and statistical results will be given in another paper.

Acknowledgements One of the authors (X. Y. Xu) is grateful to the anonymous referee whose suggestions and comments led to improvement of the manuscript. This work was funded by the National Natural Science Foundation of China (NSFC) under Grants 10221001, 10333040 and 10403003, and by NKBRFSF under Grant 20000784 and FANEDD under Grant 200226.

References

- Biskamp D., Welter H., 1989, *Sol. Phys.*, 120, 49
 Chen P. F., Fang C., Tang Y. H., Ding M. D., 1999, *ApJ*, 513, 516
 Chen P. F., Fang C., Ding M. D., Tang Y. H., 2000, *ApJ*, 520, 853
 Chen P. F., Fang C., Hu Y. Q., 2000, *Chin. Sci. Bulletin*, 45, 718
 Chen P. F., Shibata K., 2000, *ApJ*, 545, 524
 Chen P. F., Shibata K., Yokoyama T., 2001, *Earth, Planets and Space*, 53, 611
 Feynman J., Martin S. F., 1995, *J. Geophys. Res.*, 100, 3355
 Finn J. M., Guzdar P. N., Chen J., 1992, *ApJ*, 393, 800
 Guo W. P., Wu S. T., Tandberg-Hanssen E., 1996, *ApJ*, 469, 944
 Harrison R. A., 1986, *A&A*, 162, 283
 Heyvaerts J., Priest E. R., Rust D. M., 1977, *ApJ*, 216, 123
 Hu Y. Q., 1989, *J. Comput. Phys.*, 84, 441
 Kurokawa H., 1987, *Space Sci. Rev.*, 51, 49
 Kurokawa H., 1996, *IAU Colloq. 153, Magnetodynamic Phenomena in the Solar Atmosphere*, Y. Uchida, T. Kosugi, H. S. Hudson eds., Dordrecht: Kluwer, 185
 Lin J., Forbes T. G., Isenberg P. A., 2001, *J. Geophys. Res.*, 106, 25053
 Lin J., 2002, *ChJAA*, 2, 539
 Mikić Z., Linker J. A., 1994, *ApJ*, 430, 898
 Tang Y. H., Li Y. N., Fang C., 2003, *ApJ*, 534, 482
 Wang H. M., Qiu J., Jing J. et al., 2004, *ApJ*, 605, 931
 Wang Y. M., Sheeley Jr N. R., 1999, *ApJ*, 510, L157
 Wu S. T., Guo W. P., 1997, In: *Coronal Mass Ejections*, N. Crooker, J. A. Joselyn, J. Feynman eds., *Geophys. Monogr.*, 99, Washington DC: AGU, 83
 Yokoyama T., Shibata K., 1996, *PASJ*, 48, 353
 Zhang J., Dere K. P., Howard R. A. et al., 2001, *ApJ*, 559, 452
 Zhang J., Wang J. X., 2001, *ApJ*, 554, 474
 Zhang J., Wang J. X., Nitta N., 2001, *ChJAA*, 1, 85